Aerosol Science and Technology

ISSN: 0278-6826 (Print) 1521-7388 (Online) Journal homepage: https://www.tandfonline.com/loi/uast20

Inactivation of Airborne Microorganisms Using Novel Ultraviolet Radiation Sources in Reflective Flow-Through Control Devices

Kevin Ryan , Kevin McCabe , Nick Clements , Mark Hernandez & Shelly L. Miller

To cite this article: Kevin Ryan , Kevin McCabe , Nick Clements , Mark Hernandez & Shelly L. Miller (2010) Inactivation of Airborne Microorganisms Using Novel Ultraviolet Radiation Sources in Reflective Flow-Through Control Devices, Aerosol Science and Technology, 44:7, 541-550, DOI: 10.1080/02786821003762411

To link to this article: https://doi.org/10.1080/02786821003762411

Published online: 09 Jun 2010.

Aerosol Science and Technology, 44:541–550, 2010

ISSN: 0278-6826 print / 1521-7388 online
DOI: 10.1080/02786821003762411

Inactivation of Airborne Microorganisms Using Novel Ultraviolet Radiation Sources in Reflective Flow-Through Control Devices

Kevin Ryan,[1] Kevin McCabe,[2] Nick Clements,[1] Mark Hernandez,[2] and Shelly L. Miller[1]

[1]*Department of Mechanical Engineering, University of Colorado at Boulder, Boulder, Colorado, USA*
[2]*Department of Civil, Environmental, and Architectural Engineering, University of Colorado at Boulder, Boulder, Colorado, USA*

The goal of this study was to design, test, and model cylindrical flow-through control devices used to inactivate airborne microorganisms with non-mercury radiation sources and a reflective coating, through a broad relative humidity (RH) range. Bench-scale tests determined the effectiveness of three different UV-C sources—light emitting diode (LED), xenon, and mercury. In addition to measurements, modeling was performed that combined photon tracing, computational fluid dynamics, and particle tracking to predict the effectiveness of the respective UV challenges. Regardless of device configuration, UV-induced inactivation of airborne *Bacillus subtilis* and *Mycobacterium parafortuitum* was markedly sensitive to low humidity (15% RH). Actinometry measurements determined that a high reflectance wall coating increased the fluence rate by a factor of 1.6. Predictions of inactivation effectiveness using this hybrid model were in good agreement with experimental observations with errors of less than 15%.

1. BACKGROUND

Airborne diseases are transmitted by inhalation of small airborne particles, typically 1 to 5 microns in diameter, which can be generated by coughing or sneezing. As a result of a resurgence of *Mycobacterium tuberculosis* (TB) and other infectious agents that are drug resistant (Crofton et al. 1997) there has been a renewed interest in engineering controls to reduce the spread of airborne diseases. One such engineering control is a flow-through ultraviolet germicidal irradiation (UVGI) device that may reduce exposure to infectious agents.

Received 9 November 2009; accepted 12 February 2010.
Thank you to Prof. Darin Toohey at the University of Colorado at Boulder for his technical guidance and hardware support. Thank you to Luke Erickson, who helped complete the xenon lamp tests. This work was supported by a subcontract from Kansas State University.
Address correspondence to Shelly L. Miller, Department of Mechanical Engineering, Campus Box 427, University of Colorado at Boulder, Boulder, Colorado 80309-0427, USA. E-mail: Shelly.miller@colorado.edu

Ultraviolet germicidal irradiation for the inactivation of microorganisms, using UV-C radiation, has been studied since the 1940s (Sharp 1940; Luckiesh 1946). The germicidal effectiveness of UV-C is dependent on its wavelength, with the peak effectiveness at 260 nm and essentially zero at 320 nm (Koller 1952). The generally accepted mechanism of inactivation is that UV-C radiation inactivates a microorganism by damaging its deoxyribonucleic acid (DNA). This prevents microorganisms from replicating rendering them harmless (EPA 2003). UV-C wavelength, fluence rate, exposure time, temperature, and RH impact the effectiveness of UV-C irradiation inactivating microorganisms. In addition, each type of microorganism has a different response to UV-C radiation (Peccia et al. 2001).

While high efficiency particulate air (HEPA) filters are commonly used for prevention of the spread of bioaerosols in HVAC systems, flow-through UVGI control devices have some advantages over HEPA filters. Filtering can require a large pressure difference to drive air through a filter. In contrast, flow-through UVGI devices inactivate microorganisms as they flow past a light source, thus requiring no additional pressure. HEPA filters collect microorganisms on filter surfaces. These filters must be replaced regularly, which can cause disturbances to the filter and possible reintroduction of infectious agents into the environment. Conversely, flow-through UVGI control devices collect no microorganisms and their only maintenance is replacing the light source after its useful lifetime. However, sufficient UV radiation must be provided to inactivate microorganisms within typically short residence times.

Many studies have been conducted on how UVGI affects bioaerosols. Investigations have been completed on upper room systems and flow-through UVGI systems (Miller and Macher 2000; Xu et al. 2003, 2005; Ko et al. 2000; Kujundzic et al. 2007; VanOsdell and Foarde 2002). Estimates of susceptibility to UV-C radiation for a limited number of microorganisms (Xu et al. 2003; VanOsdell and Foarde 2002; Kowalski and Bahnfleth 2000; Peccia et al. 2001; Brickner et al. 2003) including viruses (Tseng and Li 2005) have been conducted.

Studies vary in their methodology when determining fluence rate. Fluence rate is the total radiant power (measured in units of power such as W) incident from all directions onto an infinitesimally small sphere of cross-sectional area dA, divided by dA (in units of area such as cm^2) (Hanovia 2009; Moes et al. 1989). Instruments, such as radiometers have been used in previous studies (Ko et al. 2000; Miller and Macher 2000). These instruments can provide an estimate of fluence rate, although they are best used for the measurement of radiation incident on flat surfaces. 360-degree photometers have also been used (Kujundzic et al. 2007). Spherical chemical actinometry best captures the UV-C fluence rate experienced by airborne microorganisms, as this technique measures incident radiation from all directions (Rahn 1997).

Fluence rate has been modeled by a number of methods including the inverse-square law (Koller 1952), radiation view factor (Siegel and Howell 1981), multiple point source summation (Jacob et al. 1970; Suidan and Severin 1986), and line source integration (Irazoqui et al. 1973) models. These models vary in their method and complexity, but all struggle with complicated geometries, and some do not take into account reflections of ultraviolet radiation. These reflections can be significant as some materials reflect a large amount of the UV-C radiation (Koller 1952).

The effectiveness of UVGI control devices has been modeled in previous studies as well. These studies combine a fluence rate model with those for determining microorganisms' exposure time in a radiation field. Recent work (Noakes et al. 2004a; Sozzi and Taghipour 2006; Munoz et al. 2007) has focused on the use of computational fluid dynamic (CFD) software to model the airflow through the UVGI device and thus determine exposure time. Using the results of this combination and a relation for the microorganisms' resistance to UVGI allows for the determination of control device effectiveness.

In this study, the effectiveness of bench-scale flow-through UVGI control devices to inactivate aerosolized microorganisms was evaluated. The UVGI control devices varied in the type of UV-C source that was used to generate the radiation, as well as wall reflectance of the surfaces internal to the device. Two prototype nontoxic UV-C sources that would have substantial environmental and operational benefits were tested, LED and xenon, as well as an industry standard low-pressure mercury vapor lamp. A proprietary high-reflectance coating was tested against bare uncoated aluminum on the wall of the control device to determine any effectiveness gain. Relative humidities of 15% and 50% were investigated. The airflow rate was also varied through the control device to change the microorganism's exposure time in the device, which ranged from 0.2 to 4 L/s. These control devices were tested on two microorganisms, *Bacillus subtilis* and *Mycobacterium parafortuitum*. These were used as surrogate organisms for airborne pathogens such as TB. Modeling incorporating computational fluid dynamics with particle and photon tracing was also applied to predict the control devices' effectiveness.

2. MATERIALS AND METHODS

2.1. Microorganisms

The control devices were tested using *Bacillus subtilis* and *Mycobacterium parafortuitum*. *B. subtilis* is a gram-positive rod, 2–3 μm in length (PS832, Popham et al. 1995). *B. subtilis* was tested in its vegetative state. *B. subtilis* was prepared from spore stock by incubating for 24 h at 37°C in 250 mL of stirring nutrient broth (Difco Laboratories). It was grown on ten nutrient agar (Difco Laboratories, Detroit, MI) plates by placing 1 mL of broth on each and grown for 48 hours at 37°C. After aerosolization and sampling, *B. subtilis* was grown on nutrient agar in an incubator at 37°C for 24 h in triplicate.

M. parafortuitum is a gram-positive rod measuring 2–4 μm in length (ATCC #19686) that has been used previously as a surrogate for TB (Xu et al. 2003). *M. parafortuitum* was prepared from −20°C stock by incubating for at least 168 h at 37°C on tryptic soy agar (Difco Laboratories, Detroit, MI). Then one colony was scraped and placed in 250 mL of stirring tryptic soy broth (Difco Laboratories, Detroit, MI) and incubated for 96 hours at 37°C. It was grown on 10 tryptic soy agar plates by placing 1mL of broth on each and grown for 72 h at 37°C. After aerosolization and sampling, *M. parafortuitum* was grown on tryptic soy agar in an incubator at 37°C for 120 h in triplicate.

2.2. Experimental Test System

2.2.1. Bioaerosol Generation and Equilibrium

Figure 1 illustrates the experimental test system including the bioaerosol generation process. Cultured cells were removed from the agar plates by aseptic scraping and suspended in 50 mL of 1× phosphate buffered saline (PBS). This solution was aerosolized using a collision six-jet nebulizer (CN25, BGI Inc., Waltham, MA) into an airtight Lucite box of approximately 1 m^3. The bioaerosol was run through a diffusion dryer (3092, TSI Inc., Minneapolis, MN) to remove excess moisture and then through a KR-85 particle-charge neutralizer (3102A, TSI Inc., Minneapolis, MN) to reduce charge. Nebulization occurred for 10 minutes under 138 kPa of filter-purified air.

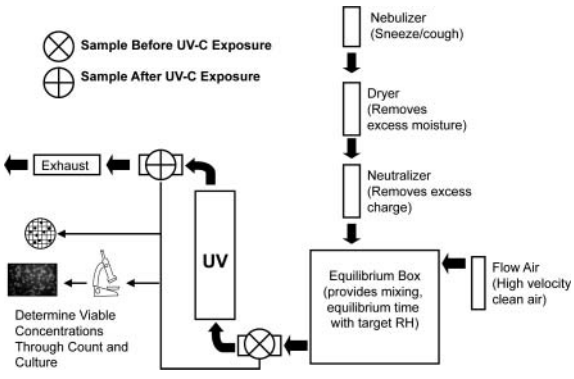

FIG. 1. Schematic of the experimental test system used to evaluate the bench-scale flow-through UVGI control devices.

The Lucite box was used to mix and equilibrate the bioaerosol to experimental conditions (RH) before UV exposure in the control device (Peccia et al. 2001). The conditions inside the box were stabilized to the desired RH by flowing dried purified air into the box for low RH tests or by operating a warm mist humidifier (CM1, Bionaire Inc., London, England) internal to the box for high RH levels. The temperature and relative humidity were measured continually during the experiments (HOBO U12, Onset Computer Corporation, Pocasset, MA). The bioaerosol was allowed to equilibrate in the box for 10 minutes while being mixed by small fans. The bioaerosol was measured with an aerodynamic particle sizer (3321 APS, TSI Inc., Minneapolis, MN) to determine its particle size distribution and mass median aerodynamic diameter (Peters and Leith 2003).

After the bioaerosol had been equilibrated, it was pushed through the control device using filtered compressed air. This airflow was set to the desired level and was verified by a wire anemometer (8475-12, TSI Inc., Minneapolis, MN) for low airflow rates and a vane anemometer (HH-30, Omega, Stamford, CT) for high airflow rates.

Airflow rates were varied from between 0.2 to 4 L/min. The relative humidity was kept within 5% of the target values of 15% and 50%. Temperature was constant at $22 +/ - 3^{\circ}$C.

2.2.2. *UVGI Control Devices*

The UVGI control devices were nominally 60 cm long and 5 cm in diameter with the lamp centered along its length. Three lamps were tested, mercury, LED, and xenon. The LED lamp was mounted on the outer radius of the control device pointed across the diameter. The mercury and xenon lamps were mounted in the center of the control device with their lengths aligned with the length of the control device. The mercury and xenon device diameters were increased to 6 cm for the center 18 cm of length to accommodate the lamp placement.

Mercury is a standard UV-C source that emits its peak wavelength at 254 nm. The lamp used in this study was a 5 W unit (TUV-PL-S 5W, Philips Inc., Amsterdam, The Netherlands) that emitted 1 W of UV-C light. Mercury lamps have been studied extensively, but they have the drawback of containing toxic material, namely mercury vapor. Therefore two new technologies were also investigated. The LED (UVTop265, Sensor Electronic Technology Inc., Columbia, SC) emitted its peak wavelength at 265 nm. Although the LED functioned, the technology was not mature. The LED was very inefficient at producing UV-C radiation ($\sim$0.5%): it required 10 W of power while only emitting 50 mW of UV-C light. Due to this inefficiency, the LED required almost 10 W of active cooling to maintain operating temperatures. The advantage of an LED lies in its solid-state construction and radiation wavelengths that can be selected at 5 nm intervals. The xenon lamp was a prototype and emitted its peak wavelength at 240 nm. This lamp was a 10 W unit and emitted approximately 1.4 W of UV-C light.

The xenon lamp was found to produce ozone. Experiments were conducted in triplicate to estimate the ozone production rate. The lamp was operated in the 1 m^3 Lucite box and ozone concentrations were monitored as a function of time using an ozone meter (202, 2B Technologies Inc., Boulder, CO). Data were interpreted according to published methods (Niu et al. 2001). The ozone concentration was also measured within the xenon control device as air flowed through the system at all applicable airflows.

In addition to varying the UV-C source, two wall reflectivities were investigated. The first was bare uncoated aluminum while the second was a proprietary high-reflectance surface coating (L2B Environmental Systems Inc., North Barrie, Ontario, Canada). The approximate reflectances at 254 nm of uncoated and coated aluminum were 75% and 90%, respectively.

2.2.3. *Aerosol Sampling*

Air samples were collected in duplicate before and after the UVGI control devices (Figure 1). Air samples were taken for one minute using liquid impingers (Biosampler, SKC Inc., Eighty Four, PA) filled with 20 mL of 1$\times$ PBS. A vacuum pump (3033, TSI Inc., Minneapolis, MN) operated the impingers at a sample rate of 12.5 L/min. A flow meter (DryCal Defender 520, Bios International Corp., Butler, NJ) was used for calibration. Prior to each experiment, all impingers were disassembled, washed with ethanol and distilled water, and autoclaved.

After sampling, direct microscopy determined the concentrations of microorganisms retained by impingers. A vacuum pulled impinger contents through 25 mm polycarbonate membrane filters (K02BPO2500, Poretics Corp., Livermore, CA) with pore diameters of 0.22 μm. Cells were stained with 4′,6-diamidino-2-phenylindole (DAPI, Research Organics, Cleveland, OH), a DNA-binding fluorescent stain. Microorganisms retained on the filter surface were mounted and examined under 1,100$\times$ magnification using an epifluorescent microscope (Eclipse E400, Nikon, Melville, NY) fitted with a mercury lamp and polarizing filters. The microorganisms were then enumerated to maintain proper solution dilution of before and after UV-C exposure samples using accepted direct microscopy methods modified for aerosol enumeration (Hernandez et al. 1999). These samples were also cultured by spiral plating (D, Spiral Biotech, Advanced Instruments Inc., Norwood, MA) on agar.

All work was performed in indirect dimmed light to control for potential photoreactivation (Peccia and Hernandez 2001). At least three replicates of each sample were plated. After incubation, all colonies were counted and the experimental surviving fraction was calculated by dividing the viable colonies exposed to UV-C by those not exposed to UV-C, under otherwise identical conditions.

2.3. Fluence Rate

The ultraviolet fluence rate was characterized spatially in the control devices using chemical actinometry (Rahn 1997). Specifically, spherical actinometry was used to measure the radiation omnidirectionally such that the radiation from both

sources and reflections was measured. The use of actinometry also allows for the spatial characterization of fluence rate.

An actinometry solution consisting of 0.6 *M* KI, 0.1 *M* KIO_3, and 0.1 *M* borate buffer at pH 9.25 was prepared. This solution was insensitive to room light and opaque to wavelengths <290 nm. This solution was used to fill actinometry spheres, custom-made from quartz to allow the transmission of the ultraviolet photons (Koller 1952). The diameters were nominally 1 cm with a variation of less than 5%. Upon exposure to photons of wavelength less than 290 nm, triiodide was formed. The amount of triiodide formed is dependent on the sphere dimensions as well as the quantum yield, which is dependent on the photon wavelength. The quantum yields were 0.73, 0.60, and 0.76 for mercury, LED, and xenon, respectively (Rahn et al. 2003).

After exposure, the actinometry solution was removed from each sphere and tested for triiodide absorption at 352 nm using a spectrophotometer (NanoDrop 1000, Thermo Scientific Inc., Wilmington, DE) along a 0.1 cm path length. The fluence rate was then found through published relations (Rahn et al. 1999).

Prior to characterizing the control device, the actinometry spheres were verified under a standard single source mercury germicidal lamp for various time periods. The results were compared with measurements made with a radiometer (1400, International Light Technologies, Peabody, MA). The actinometry and radiometry measurements agreed to within 12% on average.

Fifteen quartz actinometry spheres were arranged in the control device to find the average fluence rate. The spheres were filled with actinometry solution made fresh daily. Prior to placing the spheres inside the control device, the lamp was turned on and warmed up for a minimum of 5 min. The spheres were spaced along the interior length of the control device around the inner circumference. The actinometry spheres were placed as to minimize their shading of each other. This was accomplished by placing the spheres in a spiral pattern inside the control device. In addition, this spiral pattern was altered on each experiment to remove local results and get an average value. The 22 cm end sections of the reactor each had four spheres evenly spaced 7 cm apart. Nine spheres were spaced 2 cm apart for the center 18 cm section of the reactor. There was a greater change in fluence rate in this section due to lamp placement and the tighter spacing of the spheres provided higher resolution in this part of the UV field.

Each reactor was tested in triplicate and the results averaged to find the reactor's average fluence rate. The coefficient of variation for each device was less than 7%.

3. MODELS

3.1. Microorganism Response to UVGI

In addition to experimental work, modeling was performed to understand the microorganisms' response to UVGI. The surviving fraction of microorganisms exposed to UV-C was modeled using an exponential relationship (Koller 1952):

$$N_{uv}/N_o = S = e^{-kIt} \quad [1]$$

where

N_{uv} = number of viable microorganisms downstream of UV-C exposure
N_o = number of viable microorganisms upstream of UV-C exposure
S = surviving fraction of microorganisms after being exposed to UV-C
I = UV-C fluence rate [W/m^2]
t = UV-C exposure time [s]
k = UV-C inactivation rate [m^2/J].

Fluence (UV-C dose) is the total amount of radiant energy (expressed in units of energy such as J) from all directions incident on an infinitesimally small sphere of cross-sectional area dA, divided by dA, and is estimated by multiplying the fluence rate (I) times the exposure time (t) (Hanovia 2009). The inactivation rate constant is dependent on various factors including type of microorganism and humidity (Peccia et al. 2001). The inactivation effectiveness (E) is defined as:

$$E = 1 - S \quad [2]$$

This exponential relationship is the standard method for modeling microorganisms' response to UVGI (Kowalski and Bahnfleth 2000). Experimental data for fluence and surviving fraction were used along with the above exponential relationship to determine inactivation rate constants for *B. subtilis* and *M. parafortuitum*.

3.2. Control Device Effectiveness

Modeling was performed to predict control device effectiveness at inactivating airborne microorganisms. Modeling was separated into estimating: (1) fluence rate using a photon trace model, (2) airflow using computational fluid dynamics (CFD), and (3) microbial response and control device effectiveness.

3.2.1. Fluence Rate

A photon trace model was developed to predict the UV-C radiation field within the control devices. This model split the radiation from the UV-C source into individual photons and followed their paths as they were reflected and absorbed in the control device. Reflection was modeled as diffuse reflection due to roughness of the walls (Mahan 2002). The photons began at the source's photon emitting surface and each photon's power was diminished along their path by the percent reflected on each contact with a surface. The path of the photons ended when their power was diminished below a pre-determined threshold from multiple reflections. The lamp's power was broken into thousands of individual photons and each photon was traced through the control device. For the final model solution, ten thousand

photons were traced. The number of photons was increased until the solution converged.

The percent UV-C reflection of the control devices' interior walls was dependent on coating. The reflection off the walls was modeled as 75% for bare aluminum and 90% for the coated surface. Spherical virtual sensors throughout the control device interior then determined the local fluence rate spatially. The fluence rate at each virtual sensor was calculated by summing the incident power of each photon and dividing by the sensor's cross-sectional area. Over 10,000 virtual sensors with diameters of 5 mm were used for the final model solution. The model converged to the same solution with smaller diameter sensors, but this required additional photons and computational time. The virtual sensors were arranged throughout the control device in a radial pattern (can think of sensors as marbles poured into the control device until full). This model easily handled complex geometries, non-point source lamps, and various wall reflectivities. Calculations were executed using MatLab (MathWorks, Natick, MA).

3.2.2. *Airflow*

Commercial computational fluid dynamic (CFD) software (FLUENT 6.3.26, Ansys Inc., Canonsburg, PA) was used to model the airflow through the control device and airborne microorganisms were assumed to follow the flow due to their small size (Noakes et al. 2004b). Symmetry simplified the geometries into 2-D axisymmetric models (Figure 2). The control devices' dimensions and parameters were input (GAMBIT 2.4.6, Ansys Inc., Canonsburg, PA) and a quadrilateral mesh was constructed. The mesh was refined until the final solution was grid dependent. The model was based on Reynolds-averaged Navier-Stokes equations (Navier 1822) with a standard realizable k-epsilon turbulence model (Kundu and Cohen 2008). No slip conditions were applied to walls and all simulations were assumed to be isothermal. This type of model has been verified experimentally in previous studies to be accurate in predicting microorganisms' paths in UV devices (Noakes et al. 2006). The flow at the inlet of the control device was fully developed, and this was achieved by extending the length of the tube upstream of the control device by twice the length of the device and starting the flow as a flat profile at this artificial inlet. Simulations were carried out for all applicable flow rates by defining the mass flow rate at the inlet of the control device while the outlet was held at a constant pressure. Simulations were run until mass, momentum, and velocity residuals were approximately 10^{-6}. The airflow paths were released from the inlet of the control devices. These paths were used as the actual paths of the microorganisms through the control devices.

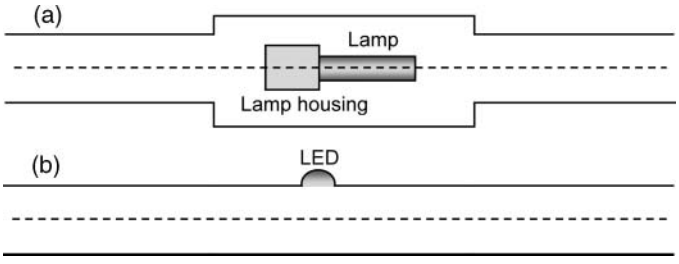

FIG. 2. Illustration (not to scale) of the 2-D axisymetric (along dashed line) model geometry for the flow-through control devices with (a) mercury and xenon lamps and (b) LEDs.

3.2.3. *Microbial Response and Control Device Effectiveness*

Combining the fluence rate and airflow models allowed for the modeling of the average fluence that microorganisms experience while passing through the control device. Integrating the spatial fluence rate over the paths of the microorganisms determined the fluence. Averaging over a set of paths gave the average fluence experienced by the microorganisms. Using the average fluence, the microorganism's inactivation rate constant as measured in the experiments, and the exponential relationship allowed for the estimation of the device effectiveness (Equation (2)).

4. RESULTS

4.1. Experiments

The data from the aerodynamic particle sizer was used to estimate the mass median aerodynamic diameter of the bioaerosols. The values were 1.1 μm for *B. subtilis* and 0.90 μm for *M. parafortuitum*. The particle size distributions of mass concentration can be seen in Figure 3.

The spatial average (+/− standard deviation (SD)) fluence rate for the coated mercury device was 33.1 +/− 1.0 W/m^2 while the uncoated device was 18.7 +/− 1.0 W/m^2. The average fluence rate for the coated LED device was 2.8 +/− 0.2 W/m^2. The average fluence rate for the coated xenon device was 35.3 +/− 1.3 W/m^2 while the uncoated device was 24.1 +/− 1.2 W/m^2. The high reflectance wall coatings increased the average fluence rate by a factor of 1.62 +/− 0.07. The reported SD is for repeat measurements and error propagation was used where appropriate.

The xenon lamp produced 25.7 +/− 1.4 mg/h of ozone. The ozone concentration in the device multiplied by the contact time (CT) was found to be 5.8 +/− 0.5 × 10^{-5} mg/L-min for all airflows due to the correlation between ozone production from the lamp and fresh air dilution from the device airflow.

The inactivation rate constants for each microorganism were estimated by plotting the surviving fraction versus fluence. The inactivation rate constants were then determined through an exponential fit using the method of least squares. The results of this analysis are presented in Figures 4–6.

T-tests (assuming unequal variance) were conducted using an alpha of 0.05 to determine statistical significance of inactivation rate constants. The inactivation rate constants of *B. subtilis* were statistically different ($p = 0.015$) at 15 and 50% RH. T-tests also verified that the inactivation rate constants of both *B. subtilis* and

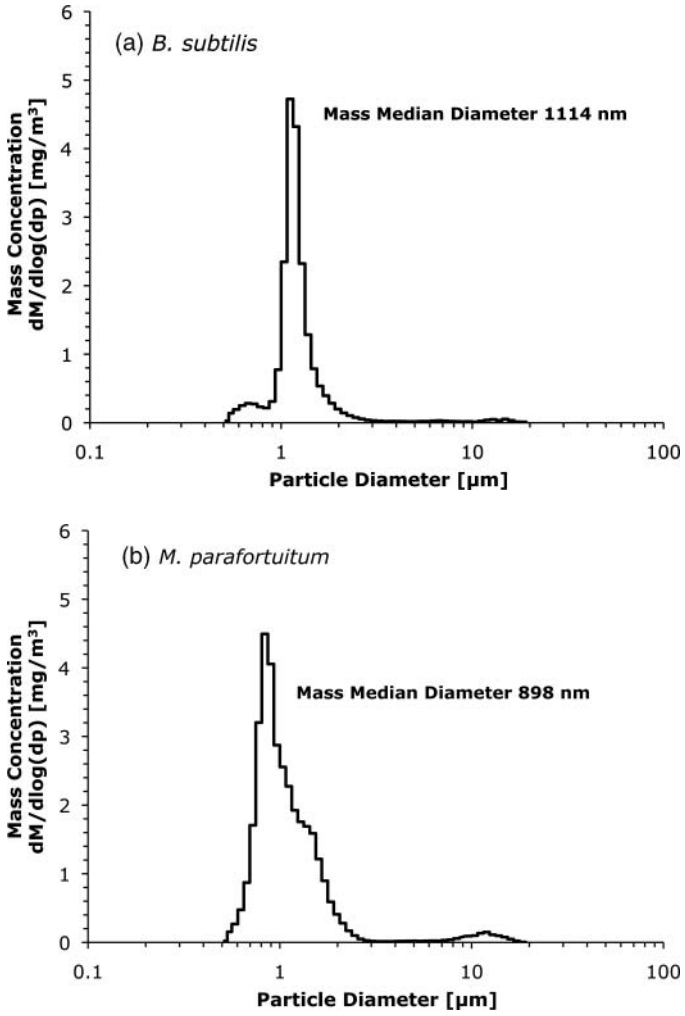

FIG. 3. Particle size distributions of mass concentration for (a) *B. subtilis* and (b) *M. parafortuitum* bioaerosol.

M. parafortuitum were not dependent on UV-C source. At 15% RH *B. subtilis* has an inactivation rate constant of 0.062 +/− 0.010 m^2/J while at 50% RH the inactivation rate constant is 21% larger at 0.077 +/− 0.026 m^2/J. At 15% RH *M. parafortuitum* has an inactivation rate constant of 0.16 +/− 0.036 m^2/J. The error in the inactivation rate constant is the standard error of the least-squares curve fit.

The results for all experiments are summarized in Table 1. This table includes the experimental scenarios, the number of each test type completed, and the average experimental effectiveness with standard deviation.

4.2. Models

Figures 7–9 compare the fluence rate as measured by actinometry and as predicted by the photon trace model. The measured and modeled average fluence rates were within 15% of each other.

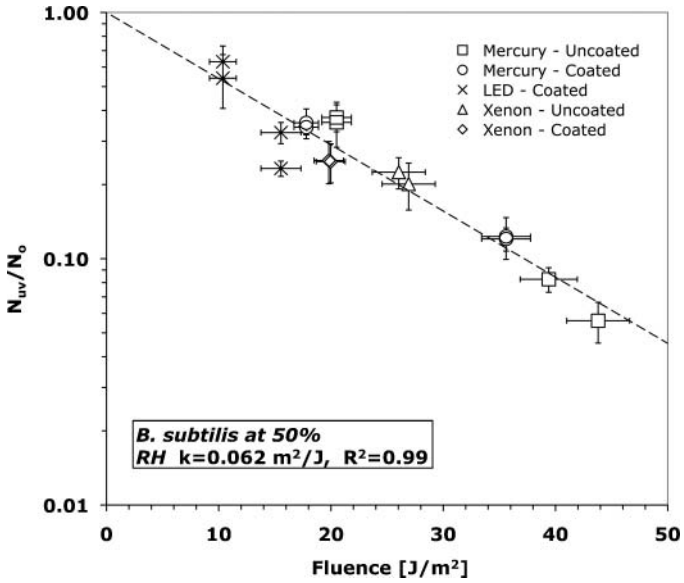

FIG. 4. Surviving fraction versus fluence for *B. subtilis* at 50% relative humidity. Error bars represent one standard deviation of the mean (n = 16).

Modeling and experimental effectiveness results agreed well with most being within 10% agreement. The results of experimental and modeled effectiveness are summarized in Table 1.

5. DISCUSSION

5.1. Experiments

This study combined widely accepted methods of testing bioaerosols and measuring fluence to determine inactivation rates. Although previous studies (e.g., Xu et al. 2003; Kujundzic

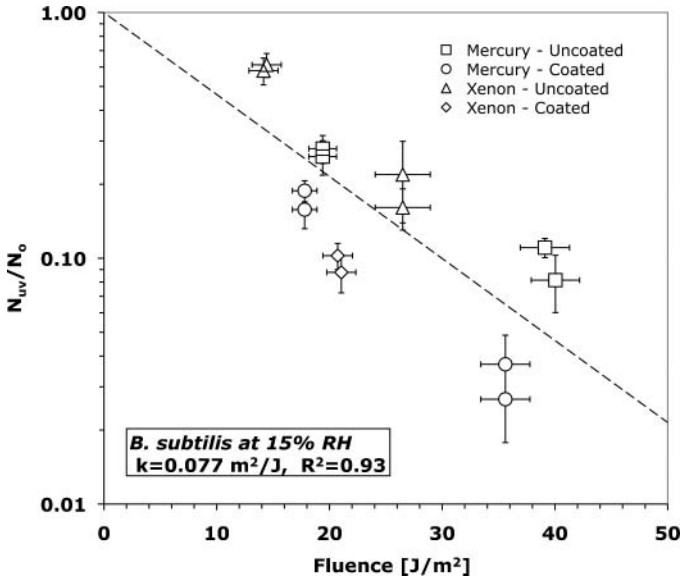

FIG. 5. Surviving fraction versus fluence for *B. subtilis* at 15% relative humidity. Error bars represent one standard deviation of the mean (n = 14).

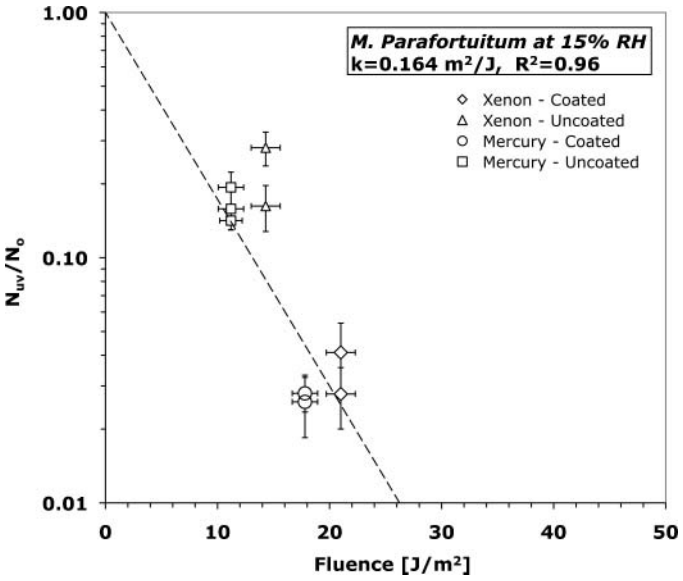

FIG. 6. Surviving fraction versus fluence for *M. parafortuitum* at 15% relative humidity. Error bars represent one standard deviation of the mean (n = 9).

et al. 2007; VanOsdell and Foarde 2002) used similar methods for producing bioaerosols, this study was careful to follow a previously reported environmental RH equilibrium protocol. The bioaerosol was allowed to achieve RH equilibrium and become well mixed for at least ten minutes before exposure to UVGI. This step assured the bioaerosol was at the specified environmental condition when tested. Previous experiments showed that bioaerosol needed an equilibration time to adapt from conditions in the nebulizer to conditions in the atmosphere in which they were being tested (Peccia et al. 2001). This modification should be considered in subsequent testing of the effects of environmental factors on bioaerosol. The aerodynamic particle sizer results for both *B. subtilis* and *M. parafortuitum* correspond well with the microorganisms' respective sizes indicating monodispersion of bacteria in the aerosol.

The xenon lamp was a significant ozone producer and most likely this would be a problem in actual applications. In this study, the concentration of ozone and the low residence time resulted in a CT of $5.8 +/- 0.5 \times 10^{-5}$ mg/L-min. Unfortunately, there are very limited studies on the direct effect of ozone on microorganisms in air. Most involve large room-scales and do not

TABLE 1
Experimental scenarios and comparison between control device effectiveness measured experimentally (average +/− SD) and modeled for UV inactivation of airborne *B. subtilis* and *M. parafortuitum*

						Effectiveness				
Microorganism	RH	Lamp	Coated	Airflow	Number of experiments	Experimental			Model*	Error**
(Type)	(%)	(Type)	(Yes/No)	(L/s)	(#)	(%)			(%)	(%)
B. subtilis	50	Mercury	Yes	4	2	65.1	+/−	2.7	64.6	–0.5
				2	2	87.8	+/−	1.4	87.8	–0.1
			No	2	2	63.4	+/−	4.4	68.7	5.3
				1	2	93.1	+/−	0.7	91.6	–1.5
		LED	Yes	0.32	2	41.4	+/−	8.3	50.9	9.4
				0.2	2	72.1	+/−	1.8	67.9	–4.2
		Xenon	Yes	4	2	75.1	+/−	3.3	67.5	–7.6
			No	2	2	78.7	+/−	2.7	72.0	–6.7
	15	Mercury	Yes	4	2	82.7	+/−	1.6	72.5	–10.2
				2	2	96.9	+/−	0.7	92.7	–4.2
			No	2	2	73.1	+/−	2.8	76.4	3.3
				1	2	90.4	+/−	1.2	95.4	5.0
		Xenon	Yes	4	2	90.5	+/−	1.0	75.3	–15.2
			No	4	2	40.4	+/−	5.0	53.7	13.3
				2	2	81.0	+/−	4.3	79.5	–1.5
M. parafortuitum		Mercury	Yes	4	2	97.3	+/−	0.4	93.6	–3.8
			No	4	3	83.6	+/−	2.5	74.4	–9.1
		Xenon	Yes	4	2	96.6	+/−	0.8	94.9	–1.7
			No	4	2	77.8	+/−	2.8	80.5	2.7

*Model used microorganism inactivation rates as follows: *B. subtilis* at 50% RH k = 0.062 (m^2/J); at 15% RH k = 0.077 (m^2/J); *M. parafortuitum* at 15% RH k = 0.164 (m^2/J).

**Error is calculated as percent difference.

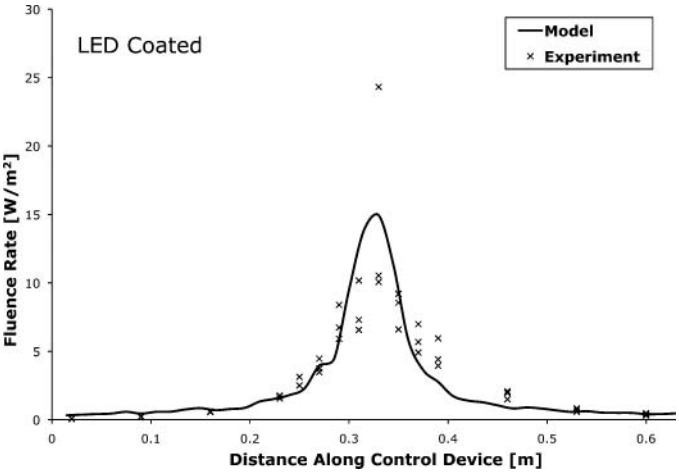

FIG. 7. The UV-C fluence rate for LED control device with coated tube walls as measured by actinometry and predicted by the photon trace model.

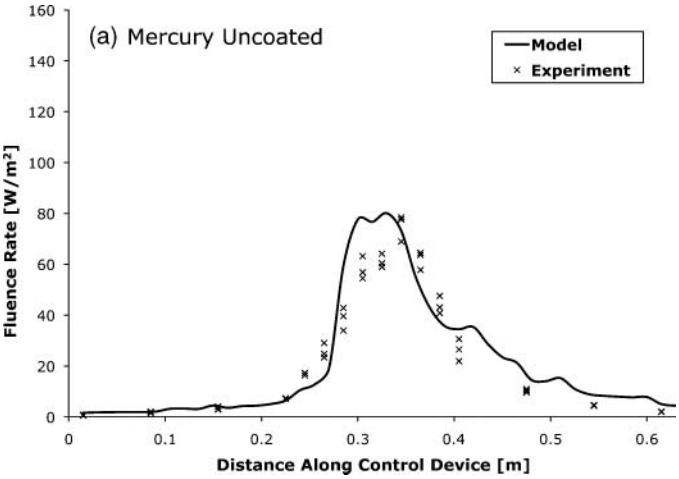

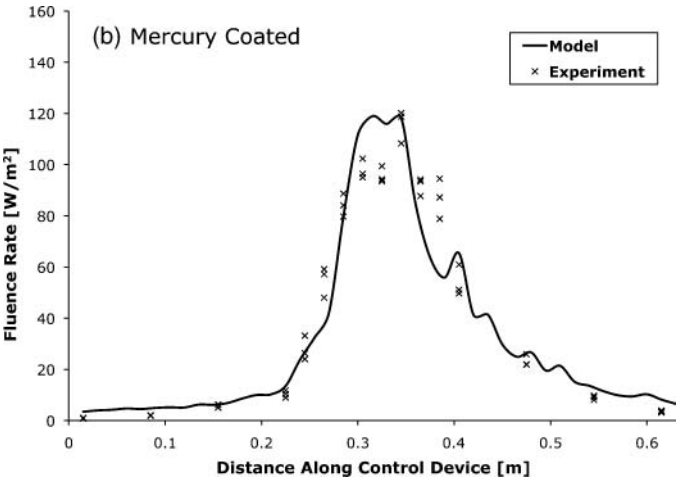

FIG. 8. The UV-C fluence rate for mercury lamp control device with (a) uncoated and (b) coated tube walls as measured by actinometry and predicted by the photon trace model.

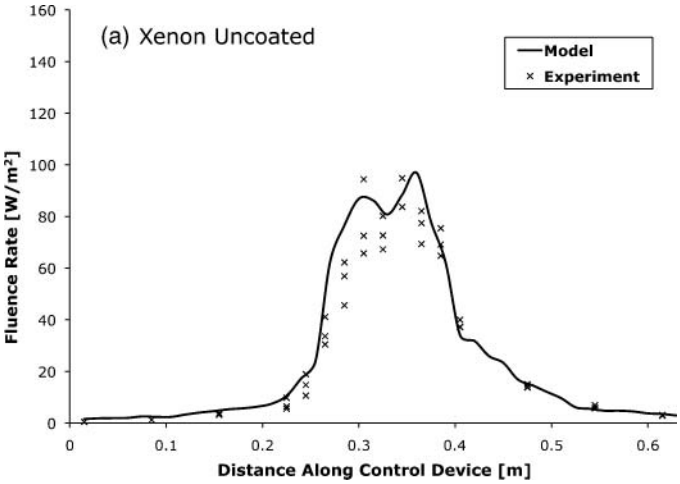

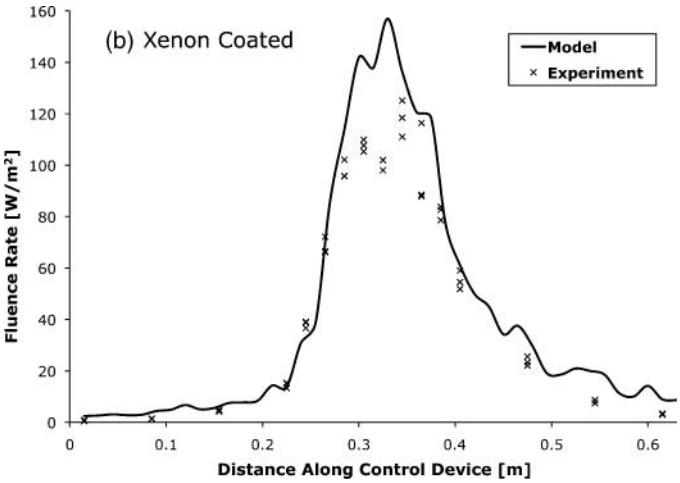

FIG. 9. The UV-C fluence rate for xenon lamp control device with (a) uncoated and (b) coated tube walls as measured by actinometry and predicted by the photon trace model.

have results that relate directly to the above exposure (CA EPA 2006). That being said, the exposure in this study was multiple orders of magnitude lower than the exposure where inactivation begins in tests conducted in air and water (Kowalski et al. 2003; EPA 1999). This low exposure most likely had no measurable inactivation on the tested microorganisms. Further, the xenon lamp tested here was a prototype and adjustments, such as changing the quartz to remove certain UV-C wavelengths, can be completed to eliminate the ozone production in future versions.

A previous study (Peccia et al. 2001) reported UV-C inactivation rates for vegetative *B. subtilis* to be 0.063 m^2/J at 40% and 0.066 m^2/J at 20% RH, respectively. These results are consistent with the trends and inactivation rate constants of 0.062 m^2/J at 50% RH and 0.077 m^2/J at 15% RH observed here. However, Peccia and co-workers used a well-mixed box for UV exposure rather than a flow-through device. *B. subtilis* spores

have been tested in a full-scale flow-through HVAC duct testing system with reported inactivation rate constants averaging 0.025 m^2/J (Van Osdell and Foarde 2002). The *B. subtilis* spores had a lower susceptibility to UVGI when compared to the vegetative *B. subtilis* tested in this study, as expected.

Higher resistance to UVGI at 50% RH when compared to 15% followed the trends reported by previous studies (Peccia et al. 2001; Tseng and Li 2005; Xu et al. 2005). The cause is most likely the additional microorganism stress at 15% RH resulting from the low moisture and also different genetic damage mechanisms at 15% as compared to 50% RH. In addition, this increased stress at 15% RH could explain the greater variation in results and thus the lower coefficient of determination of the calculated inactivation rates (Figure 5).

A previous study (Peccia and Hernandez 2001) determined the inactivation rate constant for *M. parafortuitum* to be 0.10–0.15 m^2/J at 25% RH. These values too were consistent with the inactivation rate constant of 0.164 m^2/J determined in this study at 15% RH.

Interestingly, the experimental results with different UV-C sources, and thus wavelengths, did not produce different inactivation rate constants. Although the peak wavelength different by as much as ∼10% (240 nm for xenon; 256 for LED), there is most likely overlap in the spectral output distribution of the lamps. Additional tests of each lamp's exact spectral output would be necessary to investigate this further.

This study investigated two new UV-C sources, LED and xenon, to determine their effectiveness at inactivating bioaerosols. These sources are nontoxic and may provide substantial environmental and operational benefits, but need advancement to move from prototype to production. The LED source was not powerful enough for real applications and wasted over 99% of its power input as heat, thus required active cooling to maintain operational temperatures. The xenon source required a separate igniter to light, produced ozone, and was a one-off prototype. The technology for both LED and xenon need to mature to become a viable non-toxic UV-C radiation source alternative to mercury. Once the LED and xenon prototypes improve in functionality, they may be scaled up for applications like those currently using mercury lamps, such as in heating, ventilating, and air conditioning systems or air cleaning devices.

The high-reflectance surface coating proved to increase fluence rate an average of 1.6 times when compared to uncoated aluminum. This increase in fluence rate directly benefited the control device effectiveness. A coated control device would have a higher up-front cost due to the coating procedure, but this cost may be mitigated by the higher effectiveness.

The bench-scale experimental results demonstrate that flow-through control devices inactivate airborne microorganisms efficiently, thus reducing the risk of airborne disease transmission. With further advancement in the prototypes, both xenon and LED can be scaled up to full-scale applications like those currently using mercury, such as heating, ventilating, and air conditioning systems.

5.2. Models

Previous studies showed limitations of agreement with experimental data and the simple exponential relationship model for microorganisms' response to UVGI radiation. Studies have suggested (Kowalski et al. 2001) more complicated models, but their use requires very large data sets. This limitation precluded their use in this study, but the experimental results showed the microorganisms' response to UVGI was modeled well with the simple exponential relationship with coefficient of determinations, r-squared values, above 90%.

Proper determination of fluence rate was necessary to understand UVGI and its effects. This study modeled fluence rate with a photon trace model and compared the results to fluence rate measured by spherical actinometry. The experimental and modeled average fluence rates were within 15% of each other. In future application of the photon trace model, there may be limitations, such as the computational time necessary to properly discretize and calculate the fluence rate of large control devices with complicated geometries. Computational time was not an issue for the relatively simple control devices investigated in this study, and more complicated devices would require more virtual sensors and reflective surfaces, and thus the computational time could become prohibitive. Another limitation in this study to the photon trace model was the need to split the light source into individual photons along the source's photon-emitting surface. The source manufacturers often do not provide the information necessary for this to be completed without estimations.

Models to predict control device effectiveness allow optimization of proper engineering controls to disinfect air without conducting costly experiments. Predicting effectiveness may be especially beneficial when interested in dangerous pathogens such as *Mycobacterium tuberculosis*, which present high risks with aerosol experimentation. This study combined CFD and photon tracing models with the simple exponential relationship for microorganisms' response to UVGI radiation to predict control device effectiveness. Predictions agreed well with experimental results—with errors of less than 15%. Many sources may have caused this error, including assumptions in the photon trace model, variability of microorganism response, and CFD simplifications of control device geometry and airflow equations. The ultimate limitation of this predictive method for future applications is the requirement of known inactivation rate constants for microorganisms of interest. Even with these limitations, this predictive method could be extended to alternative geometries, UV-C sources, airflows, and microorganisms with good results.

REFERENCES

Brickner, P. W., Vincent, R. L., First, M., Nardell, E., Murray, M., and Kaufman, W. (2003). The Application of Ultraviolet Germicidal Irradiation to Control Transmission of Airborne Disease: Bioterrorism Countermeasure. *Public Health Reports*. 118: 99–114.

California Environmental Protection Agency (CA EPA). (2006). *Evaluation of Ozone Emissions From Portable Indoor "Air Cleaners" That Intentionally Generate Ozone.* CA EPA Air Resources Board.

Crofton, J., Chaulet, P., and Maher, D. (1997). *Guidelines for the Management of Drug Resistant Tuberculosis,* World Health Organization, Geneva, Switzerland, pp. 5–6.

Environmental Protection Agency (EPA). (1999). *Alternative Disinfectants and Oxidants Guidance Manual.* EPA. 815-R-99-014, pp. 6–15.

Environmental Protection Agency (EPA). (2003). *Ultraviolet Disinfection Guidance Manual*. EPA. 815-D-03-007, pp. 2–6.

Hanovia. Glossary. Available at: http://www.hanovia.com/information/glossary.aspx. Accessed October 31, 2009.

Irazoqui, H. A., Cerda, J., and Cassano, A. E. (1973). Radiation Profiles in an Empty Annular Photoreactor with a Source of Finite Spatial Dimensions. *AIChE J.* 19:460–467.

Jacob, S. M., and Dranoff, J. S. (1970). Light Intensity Profiles in a Perfectly Mixed Photoreactor. *AIChE J.* 16:359–363.

Ko, G., First, M. W., and Burge, H. A. (2000). Influence of Relative Humidity on Particle Size and UV Sensitivity of *Serratia marcescens* and *Mycobacterium bovis BCG* Aerosols. *Tubercle Lung Dis*. 80:217–228.

Koller, L. R. (1952). *Ultraviolet Radiation.* John Wiley & Sons, New York, p. 8.

Kowalski, W. J., and Bahnfleth, W. P. (2000). Effective UVGI System Design Through Improved Modeling. *ASHRAE Trans*. 106:2.

Kowalski, W. J., Bahnfleth, W. P., Striebig, B. A., and Whittam, T. S. (2003). Demonstration of a Hermetic Airborne Ozone Disinfection System: Studies on E. coli. *Am. Ind. Hyg. J.* 64:222–227.

Kowalski, W. J., and Bahnfleth, W. P. (2000). UVGI Design Basics for Air and Surface Disinfection. *HPAC Eng.* 72:100–110.

Kowalski, W. J., Bahnfleth, W. P., Witham, D. L., Severin, B. F., and Whittam, T. S. (2001). Mathematical Modeling of Ultraviolet Germicidal Irradiation for Air Disinfection. *Quant. Micro*. 2:249–270.

Kujundzic, E., Hernandez, M., and Miller, S. L. (2007). Ultraviolet Germicidal Irradiation Inactivation of Airborne Fungal Spores and Bacteria in Upperroom and HVAC In-Duct Configurations. *J. Environ. Eng. Sci.* 6:1–9.

Kundu, P. K., and Cohen, I. M. (2008). *Fluid Mechanics*. American Press, California, pp. 537–598.

Luckiesh, M. (1946). *Applications of Germicidal, Erythemal, and Infrared Energy.* Van Nostrand Reinholdt Co., New York.

Mahan, J. R. (2002). *Radiation Heat Transfer, a Statistical Approach*. John Wiley & Sons, New York.

Miller, S. L., and Macher, J. M. (2000). Evaluation of a Methodology for Quantifying the Effect of Room Air Ultraviolet Germicidal Irradiation on Airborne Bacteria. *Aerosol Sci. Technol.* 33:274–294.

Moes, C. J. M., van Gemert, M. J. C., Star, W. M., Marijnissen, J. P. A., and Prahl, S. A. (1989). Measurements and Calculations of the Energy Fluence Rate in a Scattering and Absorbing Phantom at 633 nm. *Appl. Opt.* 28:2292–2296.

Munoz, A., Craik, S., and Kresta, S. (2007). Computational Fluid Dynamics for Predicting Performance of Ultraviolet Disinfection—Sensitivity to Particle Tracking Inputs. *J. Environ. Eng. Sci*. 6:285–301.

Navier, C. L. (1822). Memoire sur les lois du mouvement des fluides. Mem. *Acad. Sci. Inst. France.* 6:389–440.

Niu, J., Tung, T. C. W., and Burnett, J. (2001). Ozone Emission Rate Testing and Ranking Method Using Environmental Chamber. *Atmos. Environ*. 35:2143–2151.

Noakes, C. J., Beggs, C. B., and Sleigh, P. A. (2004a). Modeling the Performance of Upper Room Ultraviolet Germicidal Irradiation Devices in Ventilated Rooms: Comparison of Analytical and CFD methods. *Indoor Built Environ*. 13:477–488.

Noakes, C. J., Fletcher, L. A., Beggs, C. B., Sleigh, P. A., and Kerr, K. G. (2004b). Development of a Numerical Model to Simulate the Biological Inactivation of Airborne Microorganisms in the Presence of Ultraviolet Light. *J. Aerosol Sci.* 35:489–507.

Noakes, C. J., Sleigh, P. A., Fletcher, L. A., and Beggs, C. B. (2006). Use of CFD Modeling to Optimise the Design of Upper-Room UVGI Disinfection Systems for Ventilated Rooms. *Indoor Built Environ*. 15:347–356.

Peccia, J., and Hernandez, M. (2001). Photoreactivation in Airborne *Mycobacterium parafortuitum*. *Appl. Environ. Microb.* 67:4225–4232.

Peccia, J., Werth, J. M., Miller, S., and Hernandez, M. (2001). Effects of Relative Humidity on the Ultraviolet Induced Inactivation of Airborne Bacteria. *Aerosol Sci. Technol*. 35:728–740.

Peters, T. M., and Leith, D. (2003). Concentration Measurement and Counting Efficiency of the Aerodynamic Particle Sizer 3321. *J. Aerosol Sci*. 34:627–634.

Popham, D., Sengupta, S., and Setlow, P. (1995). Heat, Hydrogen Peroxide, and UV Resistance of *Bacillus subtilis* Spores with Increased Core Water Content and with or without Major DNA-Binding Proteins. *Appl. Environ. Microb*. 61:3633–3638.

Rahn, R. O. (1997). Potassium Iodide as a Chemical Actinometer for 254 nm Radiation: Use of Iodate as an Electron Scavenger. *Photochem. Photobiol.* 66:450–455.

Rahn, R. O., Stefan, M. I., Bolton, J. R., Goren, E., Shaw, P. S., and Lukke, K. R. (2003). Quantum Yield of the Iodide–Iodate Chemical Actinometer: Dependence on Wavelength and Concentration. *Photochem. Photobiol.* 78: 146–152.

Rahn, R. O., Xu, P., and Miller, S. L. (1999). Dosimetry of Room-Air Germicidal Radiation Using Spherical Actinometry. *Photochem. Photobiol.* 70:314–318.

Riley, R. L., Knight, M., and Middlebrook, G. (1976). Ultraviolet Susceptibility of BCG and Virulent Tubercle Bacilli. *Am. Rev. of Respir. Dis.* 113:413–418.

Sharp, D. G. (1940). The Effects of Ultraviolet Light on Bacteria Suspended in Air. *J. Bacteriol*. 39:535–547.

Siegel, R., and Howell, J. R. (1981). *Thermal Radiation Heat Transfer.* Taylor and Francis, New York.

Sozzi, D. A., and Taghipour, F. (2006). UV Reactor Performance Modeling by Eulerian and Lagrangian Methods. *Environ. Sci. Technol*. 40:1609–1615.

Suidan, M. T., and Severin, B. F. (1986). Light Intensity Models for Annular UV Disinfection Reactors. *AIChE J.* 32:1902–1909.

Tseng, C.-C., and Li, C.-S. (2005). Inactivation of Virus-Containing Aerosols by Ultraviolet Germicidal Radiation. *Aerosol Sci. Technol.* 39:1136–1142.

VanOsdell, D., and Foarde, K. (2002). *Defining the Effectiveness of UV Lamps Installed in Circulation Air Ductwork*. Air-Conditioning and Refrigeration Technology Institute. 21–CR/610.

Xu, P., Peccia, J., Fabian, P., Martyny, J. W., Fennelly, K. P., Hernandez, M., and Miller, S. (2003). Efficacy of Ultraviolet Germicidal Irradiation of Upperroom Air in Inactivation Airborne Bacterial Spores and Mycobateria in Full-Scale Studies. *Atmos. Environ.* 37:405–419.